



# Performance analysis of gallium nitride-based DH-HEMT with polarization-graded AlGa<sub>N</sub> back-barrier layer

Sanjib Kalita<sup>1</sup> · Bhaskar Awadhiya<sup>2</sup> · Papul Changmai<sup>3</sup>

Received: 17 February 2023 / Accepted: 11 May 2023 / Published online: 24 May 2023  
© The Author(s) 2023

## Abstract

In this paper, polarization-graded AlGa<sub>N</sub> back-barrier nanolayer has been introduced to improve the DC and RF parameters of gallium nitride-based high electron mobility transistors (HEMT). To explore the characteristics, both graded and non-graded double heterojunction high electron mobility transistor (DH-HEMT) structures are optimized using SILVACO-ATLAS physical simulator. Enhanced DC and RF parameters have been observed in the optimized graded DH-HEMT. In this paper, we have also studied the development of the quantum wells at the AlGa<sub>N</sub>/Ga<sub>N</sub> interfaces due to the conduction band discontinuity in both structures.

## 1 Introduction

Due to the high breakdown field and high mobility, AlGa<sub>N</sub>/Ga<sub>N</sub> single heterojunction high electron mobility transistors (SH-HEMT) are an excellent choice for high-frequency and high-power applications. Apart from that, due to the higher band gap of Ga<sub>N</sub>, these devices can be used at higher temperatures and voltages. Recently, few authors have theoretically reported the consequence of self-heating and different gate lengths on drain current in gallium nitride-based (Ga<sub>N</sub>) single heterojunction high electron mobility transistors (SH-HEMT) [1–3]. Again, Chattopadhyay et al. have focussed on

the effect of temperature and non-linear polarization on the gate capacitance of AlGa<sub>N</sub>/Ga<sub>N</sub> SH-HEMT [4].

The existence of aluminium nitride (AlN) nano-spacer layer in Ga<sub>N</sub>-based SH-HEMTs enhances the device performance by increasing the conduction band discontinuity [5, 6]. Piezoelectric polarization, pyroelectric properties, and other material properties are reported to raise the device performance of Ga<sub>N</sub>-based HEMTs as quantum well hetero-structures [7–11]. In addition to that, multiple HEMT structures using different semiconductor materials, such as AlGa<sub>N</sub>, InN, InAlN, etc., have been optimized by various authors to get an enhanced device performance [12–15].

Although SH-HEMTs have countless advantages, their performance may be degraded due to factors like parasitic leakage, hot electron stress, etc. To improve the performance further, a few authors reported a new HEMT structure, known as a double heterojunction high electron mobility transistor (DH-HEMT). Recently, Kalita et al. have studied different DC and RF parameters of Ga<sub>N</sub>-based SH-HEMT and DH-HEMT. From that study, it has been observed that the DC as well as RF performance upsurges in DH-HEMT [16]. It has been reported that the DH-HEMT with back barrier provides enhanced carrier confinement and better leakage protection [17]. In 2017, A. Mohanbabu et al. designed a full wave bridge inverter circuit using an enhancement mode DH-HEMT with boron-doped Ga<sub>N</sub> gate cap layer [18].

Again, despite the DH-HEMT's remarkable performances, an unwanted parasitic channel is generated at the back-barrier/buffer interface due to the existence of abrupt heterojunction. This device limitation can be overcome with

✉ Bhaskar Awadhiya  
awadhiya.bhaskar@manipal.edu

Sanjib Kalita  
sanjib.kalita25@gmail.com

Papul Changmai  
papulijec5@gmail.com

<sup>1</sup> Department of Electronics and Communication Engineering, National Institute of Technology Arunachal Pradesh, Papumpare, Jote, Arunachal Pradesh 791123, India

<sup>2</sup> Department of Electronics and Communication Engineering, Manipal Institute of Technology, Manipal Academy of Higher Education, Manipal, Udupi, Karnataka 576104, India

<sup>3</sup> Department of Electrical and Electronics Engineering, Assam Don Bosco University, District-Kamrup, Azara, Guwahati, Assam 781017, India

more advanced device design strategies that utilize polarization engineering beyond the typical abrupt-junction designs. Recently, a few authors have observed the improved device performance using polarization-graded AlGa<sub>N</sub> back-barrier nanolayer in InAlN/GaN HEMT [17].

In this work, we have introduced a new GaN-based graded DH-HEMT structure and studied different properties using two-dimensional drift–diffusion simulation. Both graded and non-graded DH-HEMTs are examined for the influence of gate length on the drain current. Moreover, in both graded and non-graded DH-HEMTs, the changes in transconductance are also investigated. The conduction band engineering is also studied in both graded and non-graded DH-HEMTs. Finally, we have examined the RF properties extracted from the simulation results for both devices.

## 2 Designs of simulated devices

As shown in Fig. 1a, b, the following are the dimensions for multiple layers of the proposed nano-electronic DH-HEMT devices: Al<sub>0.3</sub>Ga<sub>0.7</sub>N barrier layer of thickness 20 nm, 1 nm thick AlN spacer layer, main GaN channel of 59 nm, Al<sub>0.1</sub>Ga<sub>0.9</sub>N back-barrier layer of 60 nm thickness, and GaN buffer layer of 60 nm. At the bottom of the structure, 100 nm sapphire is used to provide additional mechanical strength. Apart from that, both the source and the drain have 200 nm (length) × 40 nm (height) dimensions. Gate has the

dimension of  $L_G$  (length) × 100 nm (height). The designated values of gate length ( $L_G$ ) are 0.3 and 0.5 microns. The structure has a fixed source to gate distance of 500 nm, and the gate and drain distances are variable with variations in gate length. For both the device structures, there is a fixed source to drain spacing of 1300 nm. In both structures, to reduce the current collapse, a 10 nm thick Si<sub>3</sub>N<sub>4</sub> layer is used [17]. In the non-graded HEMT structure (Fig. 1a), the Al composition is fixed as 0.1 in the AlGa<sub>N</sub> back-barrier nanolayer. In the graded HEMT structure, the Al composition is 0.1 near the GaN main channel boundary and steadily decreases to zero through the 60 nm vertical thickness of AlGa<sub>N</sub> up to the GaN buffer layer as shown in Fig. 1b. Dimensions of all the layers of proposed structures are optimized in SILVACO-ATLAS physical simulator to achieve the maximum drain current. In both cases, the doping concentration of the AlGa<sub>N</sub> layers is  $2 \times 10^{18} \text{ cm}^{-3}$ .

Normally, GaN layers are used to grow on the (000  $\bar{1}$ ) sapphire (Al<sub>2</sub>O<sub>3</sub>) substrates using molecular beam epitaxy (MBE). Similarly, the AlGa<sub>N</sub> back barrier can be grown above the GaN layer. In this paper, we have introduced a 60-nm-graded AlGa<sub>N</sub> back barrier with an Al content that changed linearly from 0% (bottom) to 10% (top). The thickness on each AlGa<sub>N</sub> layers with different Al mole fraction is of 10 nm. According to available reports, several research teams have used a variety of growing approaches to create the multi-layered devices. The multi-layered HEMT device was created in 2017 by Ren et al. using both the molecular

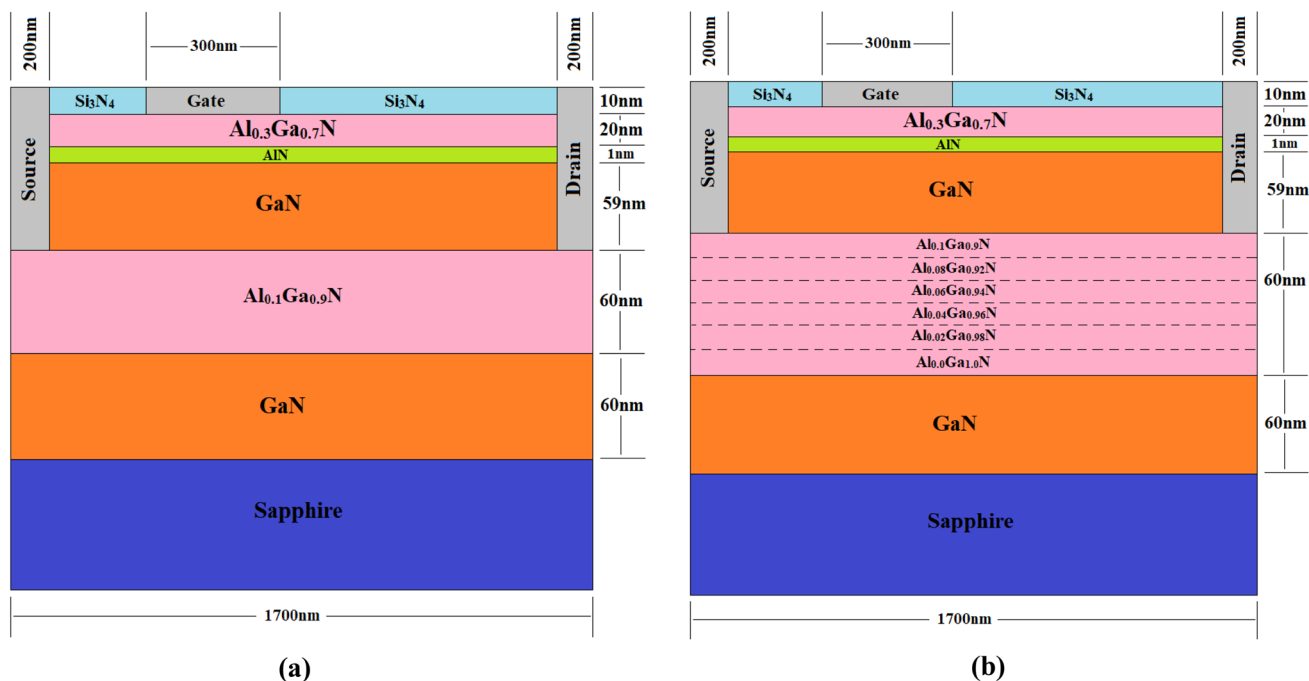


**Fig. 1** 2D structures of the nano-electronic DH-HEMT **a** with a non-graded back-barrier layer; **b** with a polarization-graded back-barrier layer. ( $L_G = 0.3 \mu\text{m}$ )

beam epitaxy (MBE) and metal organic chemical vapour deposition (MOCVD) techniques [19]. Using metal organic chemical vapour deposition (MOCVD), Zhang et al. recently created an AlGaN double-channel HEMT, and they investigated the electrical characteristics of the device [20]. Therefore, the proposed structure of this present work can be experimentally fabricated on the basis of performed simulation studies.

The idea of the proposed structure for graded HEMT is obtained from various available literature. In 2011, Das et al. designed a graded barrier AlGaN/GaN HEMT to reduce the gate leakage current. In that work, three layers of the AlGaN barrier were used with mole fractions of 0.50, 0.35, and 0.20, respectively [21]. Again, Rahman et al. optimized the graded AlInN/AlN/GaN HEMT structure to perform high-power applications [22]. In 2017, Bajaj et al. fabricated a graded nanolayer-based AlGaN/GaN HEMT including the use of a graded AlGaN channel layer [23]. Also, in 2019, Othaman et al. optimized the graded nanolayer-based HEMT with different channel materials [24]. In the same year, for X-band applications, a graded InGaN sub-channel nanolayer was introduced in the AlGaN/GaN SH-HEMT [25]. Recently, in 2020, Moon et al. studied the effect of graded AlGaN nanolayer in AlGaN/GaN HEMT and performed the linearity analysis [26]. In this present paper, to get a maximum of DC and RF performances, a graded AlGaN back-barrier nanolayer is used in the AlGaN/AlN/GaN/AlGaN/GaN DH-HEMT structure. This structure is optimized to get maximum performance. All the dimensions of this HEMT structure are based on current fabrication standards. Any change in the dimensions of this HEMT structure may result in changes in DC and RF characteristics.

In 2017, Ahmeda et al. studied the polarization and self-heating effect of AlGaN/GaN HEMT using drift–diffusion model [27]. In the same year, the self-heating effect on nano-electronic AlGaN/GaN HEMT was studied extensively by performing simulations using drift–diffusion model [28]. Again, using drift–diffusion model, the consequences of gate lengths on the cutoff frequency of HEMT were observed by Ubochi et al. [29]. In addition to that for a faster and more computationally efficient result, DD simulations can be used [30]. Therefore, according to the published literature of other authors, the drift–diffusion (DD) energy balance model is used in the simulation studies of this work which shows approximately similar results during calibration with respect to already published experimental results. Also, Monte Carlo simulation model may show better accuracy in simulation results for the nano-electronic range of HEMTs [31]. Apart from the drift–diffusion transport models, several physical models such as Fermi–Dirac, low field electron mobility, high-field mobility, Shockley–Read–Hall (SRH), and polarization have been used to simulate the proposed device. The value of trap density is  $1.1 \times 10^{11} \text{ eV}^{-1} \text{ cm}^{-2}$ .

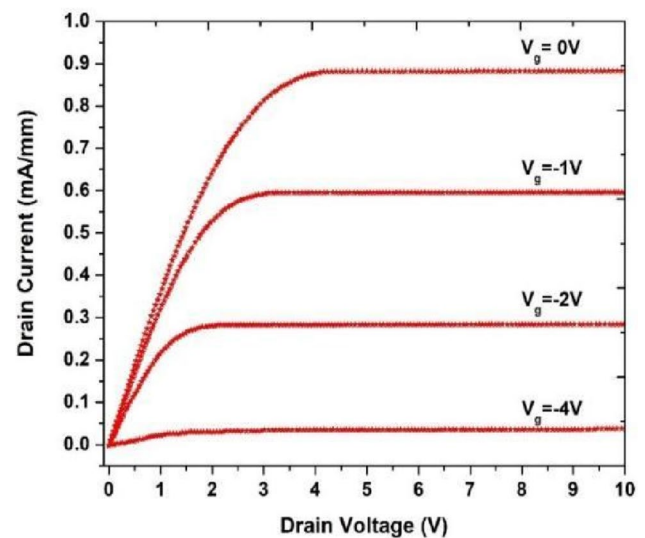


Fig. 2 Changes in drain current with respect to drain voltage at various gate voltages shown by the calibration of simulation parameters based on the already published experimental results

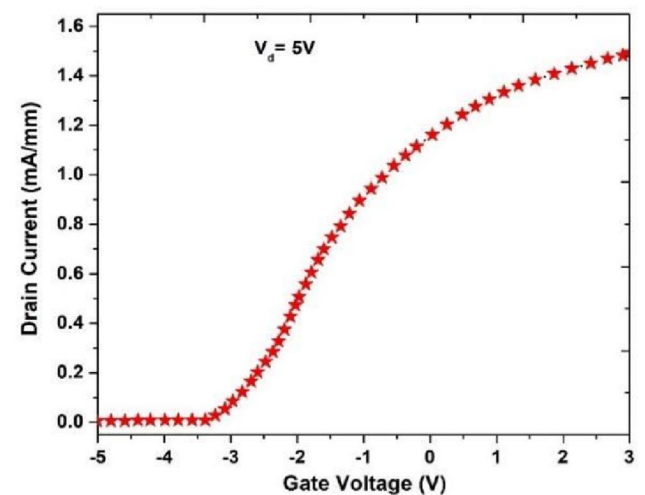


Fig. 3 Changes in drain current with respect to gate voltage at a constant drain voltage of 5 V are shown by the calibration of simulation parameters based on the already published experimental results

As the first phase of simulation studies in this work, the DH-HEMT structure is calibrated using the same structural dimensions, biasing conditions, and doping concentrations based on the published experimental results of Wang et al. [32]. Figure 2 and Fig. 3 show the changes in the drain current of calibrated HEMT structure with respect to drain voltage ( $V_d$ ) and gate voltage ( $V_g$ ), respectively. Similar DC characteristics are observed in the simulation with respect to the comparison with published experimental results [32]. All the simulation results of this research paper are obtained according to this optimized calibration in Silvaco-Atlas physical

simulator [33–35]. Hence, all the simulation results of this research paper are verified according to the already published experimental results.

### 3 Results and discussion

#### 3.1 Investigations on drain characteristics

According to Fig. 4a, at a particular gate length ( $L_G$ ) of 0.3  $\mu\text{m}$  and at any specific gate voltage ( $V_G$ ), the drain current increases with drain voltage for both non-graded HEMT and polarization-graded HEMT. It has been found that the drain current is higher in graded HEMT than in non-graded HEMT. At a gate voltage of 1 V and drain voltage of 14 V, a peak drain current of 1.3A/mm has been witnessed. Due to the presence of 2DEG, this device behaves like a normal ON device. For this reason, at greater than and equal to zero gate voltage ( $V_G$ ), a higher drain current is observed than negative gate voltage [1, 4].

Similarly, in Fig. 4b, at 0.5  $\mu\text{m}$  gate length ( $L_G$ ), the drain current rises with drain voltage in polarization-graded HEMT than in non-graded HEMT at any specific gate voltage. Again it has been observed that, both in non-graded HEMT and polarization-graded HEMT, at any specific drain voltage, the drain current is increased with respect to gate voltage ( $V_G$ ) corresponding to the 0.5  $\mu\text{m}$  gate length ( $L_G$ ) [1, 4]. As mentioned earlier, the proposed DH-HEMT structure added a 60 nm graded AlGaIn back barrier with an Al mole fraction varying from 0 to 0.1. It has been reported that a polarization-graded back barrier can counteract the

effects of parasitic channels [17]. Because of this, the confinement of 2DEG can be improved, which is advantageous for increasing the electron mobility in the channel of DH-HEMTs with graded AlGaIn back barriers. So, the increased electron mobility can result in higher current densities and quicker switching rates in the proposed DH-HEMT with a graded AlGaIn back-barrier layer.

When comparing Figs. 4a, b, it can be seen that both polarization-graded and non-graded HEMTs have greater drain currents corresponding to shorter gate lengths ( $L_G$ ). The drain current ( $I_{ds}$ ), according to a recent publication by Charfeddine et al., is stated as follows [1]:

$$I_{ds} = \frac{Z\mu\beta e}{L} \left( V_{gs} - V_{th} - \frac{V_{ds}}{2} \right) V_{ds} \quad (1)$$

where  $L$ ,  $V_{th}$ ,  $V_{gs}$ ,  $V_{ds}$ ,  $\mu$ ,  $Z$ , and  $e$  are the gate length, threshold voltage, gate voltage, drain voltage, mobility of carriers, channel width, and charge of an electron, respectively.  $\beta$  is a constant which is directly proportional to the saturation drain voltage ( $V_{dsat}$ ) [1]. Therefore, Eq. (1) states that a shorter gate length will result in a greater drain current. As a result, both polarization-graded and non-graded HEMTs show larger drain currents in our studies when the gate length ( $L_G$ ) is shorter [1]. In Fig. 4, the drain current curves are not saturating because of channel length modulation [36, 37].

According to Fig. 5a, at a specific drain voltage ( $V_D$ ) of 5 V, the drain current rises with gate voltage referring to the 0.3  $\mu\text{m}$  gate length ( $L_G$ ) in the case of both polarization-graded HEMT and non-graded HEMT [1, 4]. Again Fig. 5a shows a higher drain current in polarization-graded HEMT

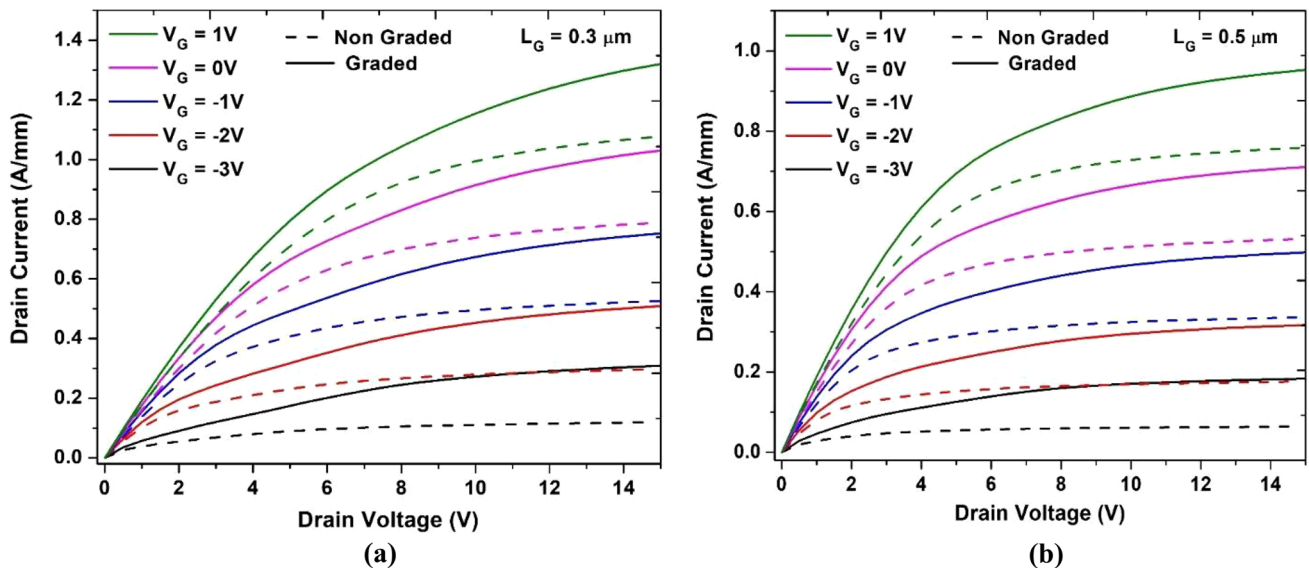


**Fig. 4** Comparative observation on V–I characteristics of non-graded HEMTs and polarization-graded HEMTs **a** at 0.3  $\mu\text{m}$  gate length ( $L_G$ ); **b** at 0.5  $\mu\text{m}$  gate length ( $L_G$ )

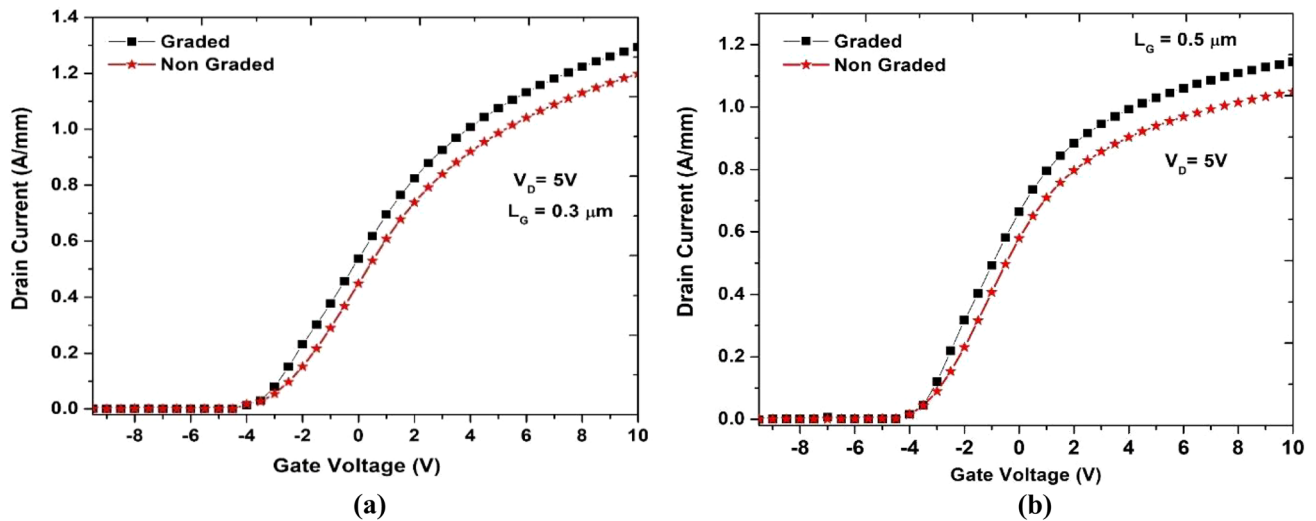


**Fig. 5** Comparative observation on transfer characteristics of non-graded HEMTs and polarization-graded HEMTs **a** at  $0.3 \mu m$  gate length ( $L_G$ ); **b** at  $0.5 \mu m$  gate length ( $L_G$ )

than in non-graded HEMT. A cutoff voltage of  $-4 V$  has been found for both polarization-graded HEMT and non-graded HEMT. Similarly, according to Fig. 5b, at  $0.5 \mu m$  gate length ( $L_G$ ), the drain current increases with gate voltage at  $5 V$  drain voltage ( $V_D$ ) in the case of both polarization-graded HEMT and non-graded HEMT [1, 4]. Additionally, Fig. 5b shows that polarization-graded HEMTs have a larger drain current than non-graded HEMTs. It has been found that a parasitic channel is formed in the GaN buffer layer of AlGaN/GaN HEMT. In Figs. 4 and 5, the drain current is higher in polarization-graded HEMTs as the effect of the

parasitic channel on 2DEG is weak in polarization-graded HEMTs than in non-graded HEMTs. Hence, the mobility of 2DEG is increased in polarization-graded HEMTs than in non-graded HEMTs.

Figure 6a presents the changes in transconductance with gate voltage at a  $0.3 \mu m$  gate length ( $L_G$ ) and fixed drain voltage ( $V_D$ ) of  $5 V$  in the case of polarization-graded HEMTs and non-graded HEMTs. Figure 6b illustrates the changes in transconductance for polarization-graded and non-graded HEMTs with a gate voltage corresponding to a  $0.5 \mu m$  gate length ( $L_G$ ) and a  $5 V$  fixed drain voltage ( $V_D$ ). When

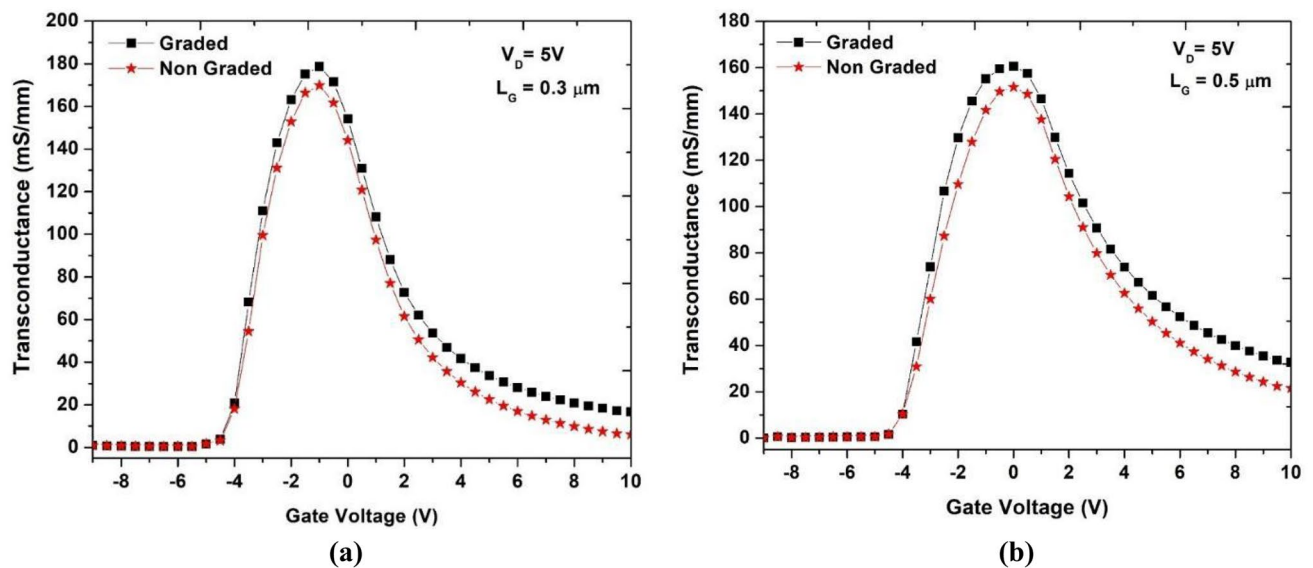


**Fig. 6** Comparative observation on variations of transconductance with a gate voltage corresponding to non-graded HEMTs and polarization-graded HEMTs **a** at  $0.3 \mu m$  gate length ( $L_G$ ), **b** at  $0.5 \mu m$  gate length ( $L_G$ )

comparing Figs. 6a, b, it can be seen that the peak transconductance for a 0.3 μm gate length ( $L_G$ ) is greater than the peak transconductance for a 0.5 μm gate length ( $L_G$ ) because for a shorter gate length, the drain current is higher. Due to the gradual Al composition in the AlGa<sub>N</sub> back-barrier layer, we can observe a weaker parasitic channel effect, which increases the mobility of the 2DEG. Increase in mobility results in higher transconductance [17].

### 3.2 Analysis of conduction band engineering and RF performance

In this work, the aluminium nitride (AlN) spacer layer is used to enhance the band gap discontinuity in HEMT structures. Figure 7a is direct evidence of the development of a quantum well for 2DEG corresponding to the non-graded HEMT and polarization-graded HEMT in the case of gate length ( $L_G$ ) of 0.3 μm. Also, Fig. 7b provides a clear illustration of the formation of a quantum well for 2DEG corresponding to the non-graded HEMT and polarization-graded HEMT in the case of gate length ( $L_G$ ) of 0.5 μm. The conduction band diagrams shown in Fig. 7 are obtained from SILVACO-ATLAS physical simulator at zero bias voltage [38]. The potential well in polarization-graded DH-HEMT is slightly deeper and wider than the conventional one. This is due to the negatively polarized field generated by the back-barrier layer, which results in better 2DEG confinement [17]. A deeper quantum well in polarization-graded HEMT structure than in non-graded HEMT structure results in higher carrier confinement. Moreover, the HEMT structure with the

shorter gate length has a greater quantum well depth. Higher carrier confinement produces a larger drain current [38].

Again, 2DEG is developed at the junction of the AlGa<sub>N</sub> and GaN layers, due to the presence of spontaneous and piezoelectric polarization in GaN-based materials. Because of this 2DEG, a quantum well is formed at this junction. The quantum well depth is related to the 2DEG sheet charge density ( $N_S$ ).

$$N_S = \frac{\epsilon(m)}{e(d + \Delta d)} \left( V_g - V_{th} - V_c - \frac{E_F}{e} \right) \tag{2}$$

where  $\epsilon(m)$  is dielectric constant,  $V_g$  is the gate voltage,  $V_C$  is the channel potential,  $d$  is the AlGa<sub>N</sub> barrier depth,  $\Delta d$  is the 2DEG mean distance from the heterointerface,  $V_{th}$  is the threshold voltage,  $E_F$  is the Fermi energy, and  $m$  is the aluminium mole fraction [39, 40]. The threshold voltage is given by,

$$V_{th} = \phi_b - \frac{\Delta E_C}{e} - \frac{eN_d d^2}{2\epsilon(m)} - \frac{|\sigma(m)|}{\epsilon(m)}(d + \Delta d) \tag{3}$$

where  $\sigma(m)$  is the total polarization,  $N_d$  is the doping concentration of AlGa<sub>N</sub> layer,  $\phi_b$  is the Schottky barrier height, and  $\Delta E_C$  is conduction band discontinuity between AlGa<sub>N</sub> layer and GaN layer [39, 40].

The frequency characteristics of designed HEMTs are shown in Figs. 8 and 9, which are extracted by the small-signal AC simulation. From Figs. 8 and 9, it has been observed that in polarization-graded HEMTs, the radio-frequency characteristics are boosted more than in

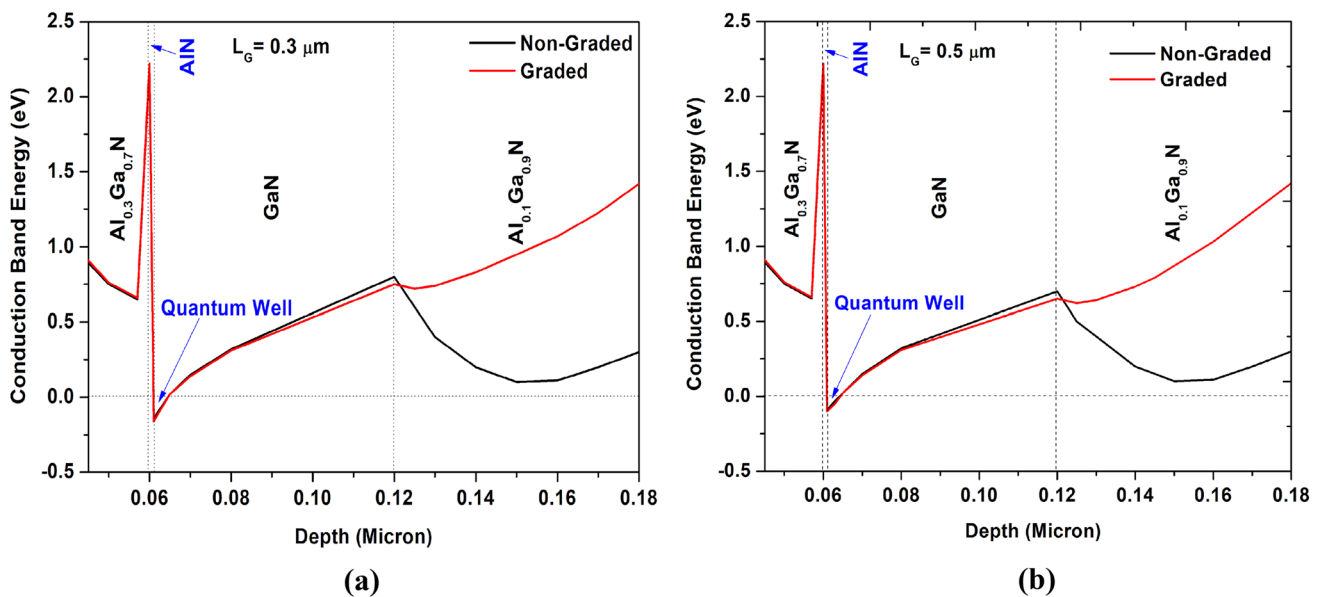
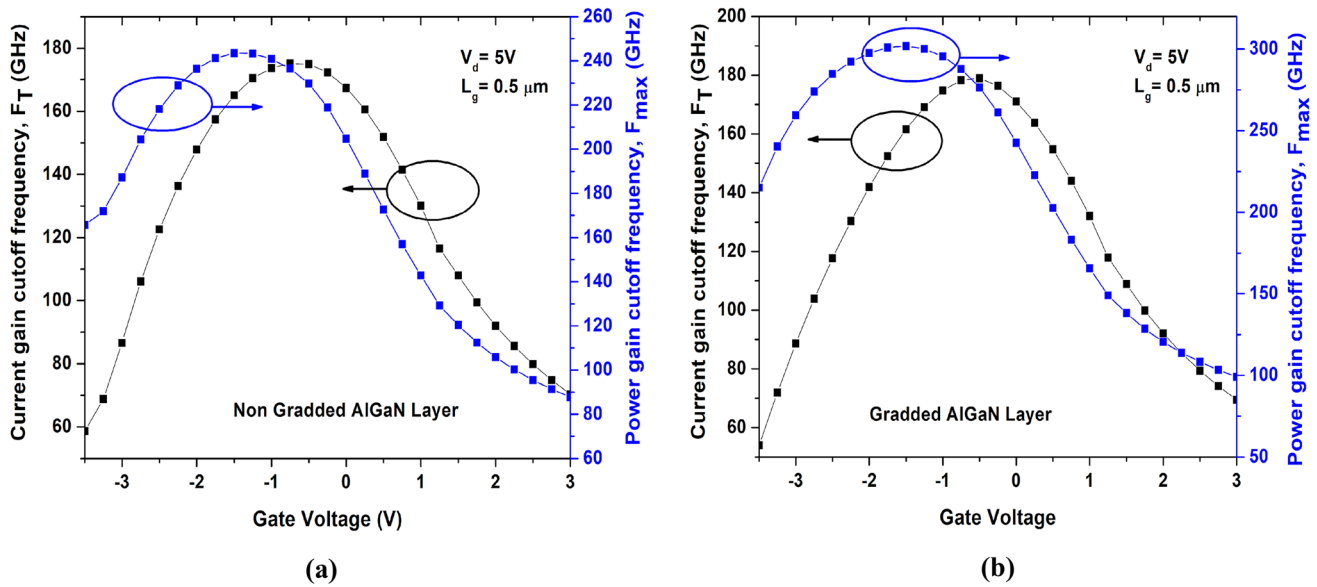


Fig. 7 Demonstration on the formation of quantum wells for 2DEG corresponding to non-graded HEMTs and polarization-graded HEMTs **a** at 0.3 μm gate length ( $L_G$ ), **b** at 0.5 μm gate length ( $L_G$ ).

These conduction band diagrams are extracted from the SILVACO-ATLAS simulation at zero bias voltage



**Fig. 8** Comparative observation on changes in current gain cutoff frequency ( $F_T$ ) and power gain cutoff frequency ( $F_{max}$ ) with respect to the gate voltage at a  $0.5 \mu\text{m}$  gate length ( $L_G$ ) and fixed drain voltage

( $V_d$ ) of  $5 \text{ V}$  **a** device having non-graded AlGaN layer; and **b** device having polarization-graded AlGaN layer

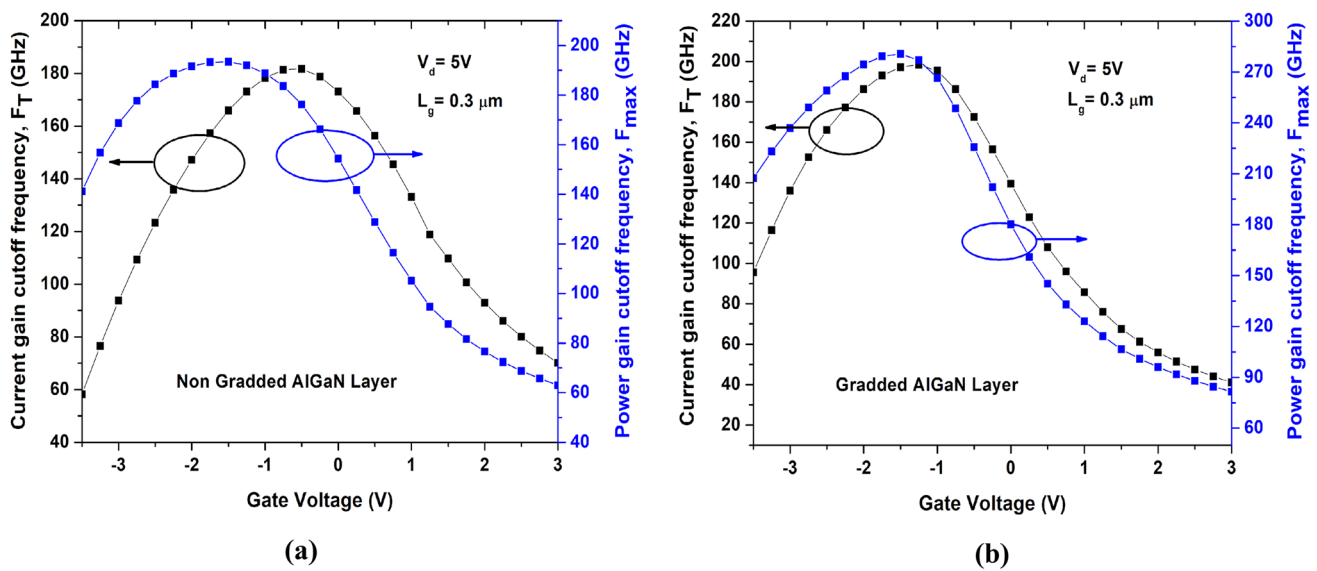


**Fig. 9** Comparative observation on changes in current gain cutoff frequency ( $F_T$ ) and power gain cutoff frequency ( $F_{max}$ ) with respect to gate voltage at a  $0.3 \mu\text{m}$  gate length ( $L_G$ ) and a fixed drain voltage

( $V_d$ ) of  $5 \text{ V}$  **a** device having non-graded AlGaN layer and **b** device having polarization-graded AlGaN layer

non-graded HEMTs. According to Fig. 8a and Fig. 8b, the current gain cutoff frequency ( $F_T$ ) rises in polarization-graded HEMT devices than in non-graded HEMT devices both having  $0.5 \mu\text{m}$  gate length ( $L_G$ ). Again, the power gain cutoff frequency ( $F_{max}$ ) also increases in polarization-graded HEMT devices than in non-graded HEMT devices both having gate length ( $L_G$ ) of  $0.5 \mu\text{m}$ .

The mathematical expressions of transconductance ( $g_m$ ), current gain cutoff frequency ( $F_T$ ), and power gain cutoff frequency ( $F_{max}$ ) are provided as follows [41],

$$g_m = \frac{\partial I_{ds}}{\partial V_{gs}} \tag{4}$$

**Table 1** Comparison amongst this present work and other recent works by different research groups

Research groups	Maximum drain current (A/mm)	Transconductance (mS/mm)	Current gain cutoff frequency ( $F_T$ ) (GHz)	Power gain cutoff frequency ( $F_{max}$ ) (GHz)
Nisha Chugh et al. [42]	0.574	398	12	77
Uiho Choi et al. [43]	0.930	233	20.1	47.6
Nisha Chugh et al. [44]	0.330	315	247	–
Yashvir Singh et al. [45]	1.3	265	20	–
This present work	1.28	181	197	205

$$F_T = \frac{g_m}{2\pi(C_{gs} + C_{gd})} \quad (5)$$

$$F_{max} = \frac{F_T}{2\sqrt{\frac{R_g + R_i + R_s}{R_{ds}} + 2\pi F_T R_g C_{gd}}} \quad (6)$$

Similarly, the current gain cutoff frequency ( $F_T$ ) is more in polarization-graded HEMT devices than in non-graded HEMT devices, as illustrated in Fig. 9. Furthermore, as shown in Fig. 9, the power gain cutoff frequency ( $F_{max}$ ) is relatively large in polarization-graded HEMT devices than in non-graded HEMT devices with gate lengths ( $L_G$ ) of 0.3  $\mu\text{m}$ . Increase in mobility results in higher transconductance. As from Eqs. (5) and (6), we can observe that the  $F_T$  and  $F_{max}$  are directly proportional to the transconductance of the device. So, in DH-HEMT with a graded AlGaIn back barrier, we have observed better current gain cutoff frequency as well as better power gain cutoff frequency. Table 1 shows the comparison amongst this present work and other recent similar works performed by different research groups.

## 4 Conclusion

Improved drain characteristics are demonstrated by two-dimensional drift–diffusion simulations. To reduce the parasitic channel (formed in the GaN buffer layer) electron concentration, an AlGaIn back-barrier layer with polarization-graded nanolayers is introduced resulting in a higher drain current. As a result, more drain current is observed in the polarization-graded HEMTs than in non-graded HEMTs. The highest drain current of 1.28 A/mm has been observed at a gate length of 0.3  $\mu\text{m}$  in polarization-graded HEMT. The higher transconductance has been observed in the HEMT structure having a shorter gate length. In polarization-graded HEMT devices, the current gain cutoff frequency is more than in non-graded HEMT devices. Furthermore, the power gain cutoff frequency in polarization-graded HEMT devices is more than in non-graded HEMT devices. As a result, the DC and AC performances of HEMTs can be improved

by employing polarization-graded AlGaIn back-barrier nanolayers.

**Author contributions** All authors contributed to the study conception and design. Material preparation, data collection and analysis were performed by [Dr. Sanjib Kalita], [Dr. Bhaskar Awadhiya], and [Dr. Papul Changmai]. The first draft of the manuscript was written by [Dr. Sanjib Kalita] and all authors commented, verified, checked, and add on value to the previous versions of the manuscript by various means. All authors read and approved the final manuscript.

**Funding** Open access funding provided by Manipal Academy of Higher Education, Manipal.

**Data availability** Not applicable.

## Declarations

**Competing interests** The authors declare no competing interests.

**Open Access** This article is licensed under a Creative Commons Attribution 4.0 International License, which permits use, sharing, adaptation, distribution and reproduction in any medium or format, as long as you give appropriate credit to the original author(s) and the source, provide a link to the Creative Commons licence, and indicate if changes were made. The images or other third party material in this article are included in the article's Creative Commons licence, unless indicated otherwise in a credit line to the material. If material is not included in the article's Creative Commons licence and your intended use is not permitted by statutory regulation or exceeds the permitted use, you will need to obtain permission directly from the copyright holder. To view a copy of this licence, visit <http://creativecommons.org/licenses/by/4.0/>.

## References

1. M. Charfeddine, H. Belmabrouk, M.A. Zaidi, H. Maaref, J. Mod. Phys. **3**, 881 (2012)
2. M.K. Chattopadhyay, S. Tokekar, Microelectron. J. **39**, 1181 (2008)
3. S. Kalita, S. Mukhopadhyay, J. Nanoelectron. Optoelectron. **13**, 1123 (2018)
4. M.K. Chattopadhyay, S. Tokekar, Solid-State Electron. **50**, 220 (2005)
5. N.M. Shrestha, Y. Li, E.Y. Chang, Jpn. J. Appl. Phys. **53**, 04EF08 (2014)
6. A. Teke, S. Gokden, R. Tulek, J.H. Leach, Q. Fan, J. Xie, U. Ozgur, H. Morkoc, S.B. Lisesivdin, E. Ozbay, New J. Phys. **11**, 063031 (2009)



7. C.H. Morko, R. Cingolani, B. Gil, *Solid-State Electron.* **43**, 1909 (1999)
8. O. Ambacher, J. Smart, J.R. Shealy, N.G. Weimann, K. Chu, M. Murphy, W.J. Schaff, L.F. Eastman, R. Dimitrov, L. Wittmer, *J. Appl. Phys.* **87**, 3222 (1999)
9. O. Ambacher, J. Majewski, C. Miskys, A. Link, M. Hermann, M. Eickhoff, M. Stutzmann, F. Bernardini, V. Fiorentini, V. Tilak, *J. Phys. Condens. Matter* **14**, 3399 (2002)
10. R.R. Pela, C. Caetano, L.G. Ferreira, J. Furthmuller, L.K. Teles, *Appl. Phys. Lett.* **98**, 151907 (2011)
11. A. Dutta, S. Kalita, S. Mukhopadhyay, *Int. J. Appl. Nanotechnol.* **5**, 26 (2019)
12. V. Janakiraman, A. Mohanbabu, S. Maheswari, A.D. Raj, S. Deb, N. VinodhKumar, *Int. J. RF Mic. Comput. Aid. Eng.* (2022). <https://doi.org/10.1002/mmce.23401>
13. A. Mohanbabu, A. Daniel Raj, S. Deb, R. Saravana Kumar, *J. Comput. Electron.* **21**, 169 (2022). <https://doi.org/10.1007/s10825-021-01816-2>
14. A. Mohanbabu, N. Mohankumar, D. Godwin Raj, P. Sarkar, *Phys E Low-Dimens. Syst. Nanostruct.* **92**, 23 (2017). <https://doi.org/10.1016/j.physe.2017.05.005>
15. A. Mohanbabu, N. Mohankumar, D. Godwin Raj, P. Sarkar, S.K. Saha, *Superlattice. Microstruct.* **103**, 270 (2017). <https://doi.org/10.1016/j.spmi.2017.01.043>
16. A. Dutta, S. Kalita, S. Mukhopadhyay, *Opt. Quant. Electron.* **53**(2), 1 (2021)
17. Gu. Yan, D. Chang, H. Sun, J. Zhao, G. Yang, Z. Dai, Yu. Ding, *Electronics* **8**, 885 (2019)
18. A. Mohanbabu, N. Mohankumar, D. Godwin Raj, P. Sarkar, S.K. Saha, *Int. J. Numer Model* (2017). <https://doi.org/10.1002/jnm.2276>
19. F. Ren, S.J. Pearton, S. Ahn, Y.H. Lin, F. Machuca, R. Weiss, A. Welsh, M. McCartney, D. Smith, I.I. Kravchenko, *ECS J. Solid State Sci. Technol.* **6**(11), S3078 (2017)
20. Y. Zhang, Y. Li, J. Wang, Y. Shen, L. Du, Y. Li, Z. Wang, S. Xu, J. Zhang, Y. Hao, *Nanoscale Res. Lett.* **15**, 114 (2020)
21. P. Das, D. Biswas, *J. Nano- Electron. Phys.* **3**, 972 (2011)
22. S. Rahman, N.A.F. Othman, S.W.M. Hatta, N. Soin, *ECS J. Solid-State Sci. Technol.* **6**(12), P805 (2017)
23. S.H. Sohel, A. Xie, E. Beam, H. Xue, T. Razzak, S. Bajaj, Y. Cao, C. Lee, W. Lu, S. Rajan, *IEEE Electron Device Lett.* **40**(4), 522 (2019)
24. J. S. Moon, B. Grabar, M. Antcliffe, J. Wong, C. Dao, P. Chen, E. Arkun, I. Khalaf, A. Corrion, J. Chappell, N. Venkatesan, P. Fay, 2020 IEEE/MTT-S International Microwave Symposium, p. 573 2020
25. S. Bajaj, Z. Yang, F. Akyol, P.S. Park, Y. Zhang, A.L. Price, S. Krishnamoorthy, D.J. Meyer, S. Rajan, *Hfhydyfytjt jyutffyt jtyfyuft. IEEE Trans. Electron. Devices* **64**(8), 3114 (2017)
26. N.A.F. Othman, S. Rahman, *Microelectron. Int.* **36**(2), 73 (2019)
27. K. Ahmeda, B. Ubochi, B. Benbakhti, S.J. Duffy, A. Soltani, W.D. Zhang, K. Kalna, *IEEE Access* **5**, 20946 (2017)
28. B. Ubochi, K. Ahmeda, K. Kalna, *ECS J. Solid. State Sci. Technol.* **6**(11), S3005 (2017)
29. B. Ubochi, S. Faramehr, K. Ahmeda, P. Igić, K. Kalna, *Microelectron. Reliab.* **71**, 35 (2017)
30. F. Soroush, K. Karol, I. Petar, *Semicond. Sci. Technol.* **29**, 025007 (2014). <https://doi.org/10.1088/0268-1242/29/2/025007>
31. S. Sinha, K.E. Goodson, *Int. J. Multiscale Comput. Eng.* **3**(1), 107 (2005)
32. X. Wang, G. Hu, Z. Ma, J. Ran, C. Wang, H. Xiao, J. Tang, J. Li, J. Wang, Y. Zeng, J. Li, Z. Wang, *J. Cryst. Growth* **298**, 835 (2017)
33. B. Awadhiya, S. Pandey, K. Nigam, P. Kondekar, *Superlattice. Microst.* **111**, 293 (2017)
34. S. Yadav, B. Awadhiya, A. Mittal, *SILICON* (2022). <https://doi.org/10.1007/s12633-022-01905-2>
35. B. Awadhiya, S. Yadav, Acharya, *SILICON* (2022). <https://doi.org/10.1007/s12633-022-02053-3>
36. D.K. Panda, T.R. Lenka, *J. Semiconduct.* **38**(6), 64002 (2017)
37. E.N. Ganesh, *Int. J. Emerg. Trends Technol. Comput. Sci.* **2**(1), 123 (2013)
38. S. Mukhopadhyay, *J. Semiconduct. Devices Circuit.* **4**, 6 (2017)
39. S. Rabbaa, J. Stiens, *J. Phys. D Appl. Phys.* **44**, 325103 (2011)
40. S. Rabbaa, J. Stiens, *Proceedings of IEEE-ICSE2012* (IEEE, Kuala Lumpur, Malaysia, 2012), p.374
41. B. Hou, L. Yang, M. Mi, M. Zhang, C. Yi, M. Wu, Q. Zhu, Y. Lu, J. Zhu, X. Zhou, L. Lv, X. Ma, Y. Hao, *J. Phys. D Appl. Phys.* **53**, 145102 (2020)
42. C. Nisha, M. Kumar, M. Bhattacharya, R.S. Gupta, *Semiconductors* **53**(13), 1784 (2019)
43. U. Choi, H.-S. Kim, K. Lee, D. Jung, T. Kwak, T. Jang, Y. Nam, B. So, M.-J. Kang, K.-S. Seo, M. Han, S. Choi, S. Lee, H.-Y. Cha, O. Nam, *Phys. Status Solidi A* **217**, 1900695 (2020). <https://doi.org/10.1002/pssa.201900695>
44. N. Chugh, M. Bhattacharya, S.S. Manoj Kumar, R.S. Deswal, Gupta, *Sbjkhsne ljjd;klrj asfsuh. J. Comput. Electron.* (2018). <https://doi.org/10.1007/s10825-018-1190-0>
45. Y. Singh, M. Payal, *Conference on advances in communication and control systems 2013 (CAC2S 2013)* (Atlantis Press, 2013), p.222

**Publisher's Note** Springer Nature remains neutral with regard to jurisdictional claims in published maps and institutional affiliations.